

Boundary Vorticity Flux and Engineering Flow Management

Jiezhi Wu^{1,2,*}, Hong Wu³ and Qiushi Li³

¹ State Key Laboratory for Turbulence and Complex Systems, College of Engineering, Peking University, Beijing, 100871, China

² The University of Tennessee Space Institute, Tullahoma, TN 37388, USA

³ National Key Laboratory on Aero-engines School of Jet Propulsion, Beihang University, Beijing, 100083, China

Received 01 December 2008; Accepted (in revised version) 16 January 2009

Available online 22 April 2009

Abstract. To improve the performance of complex viscous engineering flows, the focus should be on local dynamics (local processes and structures) measured by the space-time derivatives of the primary-variable fields, rather than these fields themselves. In the context of optimal flow management such as optimal configuration design and flow control, the local fluid dynamics on solid wall is of most direct relevance. For large Reynolds-number flows, we show that the on-wall local dynamics is highlighted by the balance between tangential pressure gradient and vorticity creation rate at the wall (boundary vorticity flux, BVF), namely the on-wall coupling of the compressing and shearing processes. This basic concept is demonstrated by previously unpublished and newly obtained numerical examples for external and internal flows, including the role of BVF as a faithful marker of the local appearance of boundary-layer separation and wall curvature discontinuity, and the use of BVF-based formulas to optimize the integrated performance of airfoil and compressor rotor blade.

AMS subject classifications: 76D17, 76D55, 76N25, 76G25

Key words: Aerodynamics, boundary vorticity flux, optimal design.

1 Introduction

Any practical external or internal engineering flow has a set of global performances as its design objectives, e.g., the lift and drag of a wing or the pressure ratio and efficiency of a compressor, as well as the operational stability of the flow. Ever since

*Corresponding author.

URL: <http://lscs.pku.edu.cn/cn/Article.asp?ArticleId=95>

Email: jzwu@coe.pku.edu.cn (J. Z. Wu), whbuaa@sjp.buaa.edu.cn (H. Wu), Liqs@buaa.edu.cn (Q. S. Li)

Helmholtz [3] realized for the first time the crucial importance of local vortical structures measured by the vorticity in practical flows, it has now been well recognized that all global performances of engineering flows are dominated by various local dynamic structures, such as boundary layers, free shear layers, vortices, turbulent coherent structures, shock waves and other nonlinear waves. In a multi-dimensional, viscous and compressible flow, the local structures as exemplified above come from three fundamental dynamic processes [1, 5]: the (transverse) *shearing process*, the (longitudinal) *compressing process* and the *thermal process*. The first two processes are the fundamental bulk dynamic processes in fluid motion. They are measured by the vorticity field and dilatation-pressure field (or other proper scalar field) and their characteristic behaviors are governed by the Reynolds number and Mach number, respectively. These two fundamental processes are inherently coupled both in the interior of the flow field via the nonlinear terms of the governing equations and on flow boundary via the adherence condition. In addition, the thermal process is inevitably involved as long as the flow is compressible. It can be conveniently measured by the entropy gradient field which is inherently coupled with both compressing and shearing processes. This is why modern physical theories, experiments and computations on complex flows have been focusing on the nonlinear evolutions and interactions of these local structures. Naturally, a deep and quantitative physical understanding of these structures and their role in global flow performance has become the very basis of *optimal flow management* including configuration design and flow control.

As seen above, any of the local structures are measured not by primary variables themselves (e.g., velocity \mathbf{u} , pressure p and entropy s) but their spatial-temporal derivatives, which appear in the local balances of mass, momentum and energy, and thereby interact each other to produce various dynamic effects, especially the aerodynamic force. Indeed, a uniform (\mathbf{u}, p) field produces no force at all; a wing experiences a pressure force only if p varies over its surface. Dynamically, the pressure field itself can only be related to the kinetic energy via the Bernoulli equation, which however exists only when the flow is circulation-preserving, and merely reflects the dynamics of longitudinal (compressing) process [11][†]. Circulation is no longer preserving in generic viscous shear flows.

There have been various theories on global flow performance in terms of local structures in both external and internal aerodynamics, which are systematically presented by Wu, Ma & Zhou [11], Wu, Lu & Zhuang [10] and Yang et al. [18, 19]. While all these theories may enhance our physical understanding of the flow structures in their different evolution stages and their relevance to global performances, they are not equally useful in flow management, which depends directly and critically on the *local dynamics right on the solid boundaries*. A solid wall is the ultimate root of all flow structures that in turn leave signature thereon. The management of these on-wall root and signature, therefore, is of particular importance in the improvement of global flow

[†]In a circulation-preserving flow, the shearing process appears in a series of vorticity conservation theorems. It is coupled with the compressing process only through the vorticity-induced velocity that contributes to the kinetic energy.

performance. As just said, the on-wall distribution of primary variables[‡] does not capture local dynamics; but their space-time variations do. This is what one should focus in on-wall flow diagnosis and management. Then, as will be shown below, at least for flows at large Reynolds numbers, the central concept of the on-wall local dynamics is the *boundary vorticity flux* (BVF) pioneered by Lighthill [6].

The theory of BVF has also been extensively studied and reviewed (e.g., [11–15]). In this paper we provide renewed insight to its central role in the on-wall local dynamics, to the physics of how the BVF peaks are related locally to the sudden change of wall conditions and globally to the pressure force and moment. We then report some applications of BVF to the optimal design in practical external and internal flows. The characteristic Reynolds number Re is assumed very large or even approaching infinity.

2 On-wall dynamics and boundary vorticity flux

Let $\mathbf{a}=D\mathbf{u}/Dt$ be the material acceleration, $\vartheta=\nabla \cdot \mathbf{u}$ be the dilatation, $\boldsymbol{\omega}=\nabla \times \mathbf{u}$ be the vorticity, and μ and ζ be the shear and bulk viscosities, respectively, both being assumed constant for simplicity. The Navier-Stokes (NS) equation for a viscous compressible flow of unit volume can be written as a *natural Helmholtz decomposition* of the inertial force $\rho\mathbf{a}$ [8, 11]:

$$\rho\mathbf{a} = -\nabla\Pi - \nabla \times (\mu\boldsymbol{\omega}), \tag{2.1}$$

where

$$-\Pi = -p + \mu_\theta\vartheta, \tag{2.2}$$

is the normal stress consisting of the pressure and a viscous-dilatation correction with

$$\mu_\theta \equiv \zeta + 4\mu/3, \tag{2.3}$$

known as the *longitudinal viscous coefficient* (see, e.g., [4]). Eq. (2.1) indicates that locally the inertial force $\rho\mathbf{a}$ is balanced by the compressing process Π and shearing process $\mu\boldsymbol{\omega}$. The basis of the on-wall dynamics is nothing but the application of (2.1) on a solid wall ∂B of normal \mathbf{n} (pointing out of the fluid) and use of a corollary of the adherence condition, $\mathbf{a}=\mathbf{a}_B$, where \mathbf{a}_B is the known acceleration of the wall. This on-wall equation can be split into a pair of *normal-tangent* ($\boldsymbol{\omega}, \Pi$) couplings:

$$-\frac{1}{\rho} \frac{\partial \Pi}{\partial n} = \mathbf{n} \cdot \mathbf{a}_B + v(\mathbf{n} \times \nabla) \cdot \boldsymbol{\omega}, \tag{2.4a}$$

$$v \frac{\partial \boldsymbol{\omega}}{\partial n} = \mathbf{n} \times \mathbf{a}_B + \frac{1}{\rho} \mathbf{n} \times \nabla \Pi + v(\mathbf{n} \times \nabla) \times \boldsymbol{\omega}, \tag{2.4b}$$

where $v=\mu/\rho$ and $\mathbf{a}, \Pi, \boldsymbol{\omega}$ on the right-hand side all take their on-wall values.[§]

[‡]On a solid wall, roughly speaking, the velocity \mathbf{u} is replaced by the shear stress $\boldsymbol{\tau}$.

[§]For two-dimensional flow the last term on the right-hand side of (2.4b) vanishes.

Except for extremal conditions where the variation of μ and μ_θ as temperature is significant, (2.4a) and (2.4b) are exact and sufficiently general for all viscous incompressible and compressible flows, steady or unsteady. If a flow field is to be solved from the NS equations, (2.4a) is the basis of formulating a Neumann condition for Π or pressure, while (2.4b) is the basis of formulating a Neumann condition in the vorticity-based schemes to exclude possible spurious solution caused by rising the order of the equation [11]. On the other hand, in flow diagnosis and management, one's concern is usually focused on the most dominant mechanisms only, and hence it is important to identify the relative importance of (2.4a) and (2.4b) which varies as the Reynolds number. This paper considers $Re = \rho UL / \mu \gg 1$ only, where U and L are characteristic velocity and length. Viewing (2.4) as having been nondimensionalized, then generically there is $|\omega| = \mathcal{O}(Re^{1/2})$. Along with the fact that $\mathbf{n} \times \nabla$ is an $\mathcal{O}(1)$ operator, the explicit viscous terms on the right-hand side of (2.4a) and (2.4b) are both of $\mathcal{O}(Re^{-1/2}) \ll 1$. Thus, in (2.4a) the normal gradient of Π is dominated by the normal wall acceleration; while in (2.4b) the viscous *boundary vorticity flux* (BVF) $v \partial \omega / \partial n \equiv \sigma$ is dominated by the tangent pressure gradient and wall acceleration. Note that on a fluid surface element inside the flow, σ is merely a measure of how much vorticity is diffused from one side of the surface to another; but on a solid boundary it measures how much vorticity is *newly created* per unit area in unit time [6].

The wall acceleration \mathbf{a}_B in (2.4) is important mainly for unsteady flows with flexible boundaries, such as in nonlinear aeroelasticity, animal locomotion in air and water, as well as flow controls by flexible walls. Of this kind of flow controls see, e.g., the turbulent friction reduction by flexible wall which makes spanwise oscillation that forms tangent traveling waves in $\mathbf{n} \times \mathbf{a}_B$ to control the BVF [20], and wake-vortex elimination by flexible wall which makes up-down oscillation that forms a traveling wave in $\mathbf{n} \cdot \mathbf{a}_B$ to control the normal pressure gradient [9]. The theory for the fluid kinematics at a generic deformable wall is given by Wu et al. [16].

Having made the above general remarks on the normal-tangent (ω, Π) coupling on the wall, this paper will be confined to flow over a rigid surface, for which \mathbf{a}_B can be made disappear by working in the frame of reference fixed to the body. To further focus on the key physics at large Re and for the neatness of presentation, in what follow we often neglect the $\mathcal{O}(Re^{-1/2})$ viscous terms. Thus the entire $\partial \Pi / \partial n$ in (2.4a) and $v(\mathbf{n} \times \nabla) \times \omega$ in (2.4b) are negligible, but *the BVF is always of $\mathcal{O}(1)$ even if $Re \rightarrow \infty$* .[¶] Consequently, we have

$$\sigma \equiv v \frac{\partial \omega}{\partial n} \simeq \sigma_p \equiv \frac{1}{\rho} \mathbf{n} \times \nabla p, \quad (2.5)$$

which highlights the on-wall dynamics at large Re where the BVF plays a dual role. On the one hand, the tangent pressure gradient in (2.5) is a result or on-wall signature

[¶]Numerical examples (not shown here) have confirmed that the viscous term on the right-hand side of (2.4b) is indeed as small as $\mathcal{O}(Re^{-1/2})$. On the other hand, on a stationary wall, $\Pi \neq p$ only if the flow is unsteady, where their difference $\mu_\theta \vartheta$ is generically still small, perhaps except inside some oscillating shock layers.

of the entire fluid motion, which measures the local dynamics of compressing process. On the other hand, once that tangent pressure gradient is formed on the wall, it becomes a cause or on-wall root of new vorticity, which measures the local dynamics of the shearing process. Therefore, in a generic viscous flow over a stationary wall at large Re the local balance between the vorticity creation rate and tangent pressure gradient stands at the center of the entire on-wall dynamics.

Note that the entropy gradient effect has been included implicitly in (2.1), (2.4), and (2.5). This effect can be seen explicitly if we replace (2.1) by the Crocco-Vazsonyi equation (per unit mass):

$$\frac{\partial \mathbf{u}}{\partial t} + \boldsymbol{\omega} \times \mathbf{u} = -\nabla H + T\nabla s + \nu_{\theta} \nabla \vartheta - \nu \nabla \times \boldsymbol{\omega}, \tag{2.6}$$

where $H=h + |\mathbf{u}|^2/2$ is the total enthalpy and $\nu_{\theta}=\mu_{\theta}/\rho$. Thus, after dropping explicit viscous terms except the BVF of $\mathcal{O}(1)$, there is the normal-tangent $(\boldsymbol{\omega}, h)$ couplings

$$-\frac{\partial h}{\partial n} \simeq \mathbf{n} \cdot \mathbf{a}_B - T \frac{\partial s}{\partial n}, \tag{2.7a}$$

$$\nu \frac{\partial \boldsymbol{\omega}}{\partial n} \simeq \mathbf{n} \times (\mathbf{a}_B + \nabla h - T\nabla s). \tag{2.7b}$$

This pair of on-wall dynamic equations can be used as alternative to (2.4), depending on which is more convenient. In the rest of this paper we just work with (2.5).

3 BVF and boundary layer separation

One of the key issues in complex flow diagnosis is to predict when and where a boundary layer will separate, a key process that may considerably alter global flow performance. The BVF, especially its pressure-gradient constituent σ_p , is a good marker to signify the separation is happening.

The physical reason for this important role of σ_p is explained by the triple-deck theory (cf. [11], § 5.3). This theory reveals that in the boundary-layer separation zone there must appear a local *interactive pressure* of $\mathcal{O}(Re^{-1/4})$ across the separation line, which alters the parabolic nature of the boundary-layer approximation to a locally elliptic nature of the triple-deck equations, and thereby eliminates the singularity of the former. Although when $Re \gg 1$ this interactive pressure is as small as $\mathcal{O}(Re^{-1/4})$ and hard to be detected in numerical simulation, the width of the separation zone is of only $\mathcal{O}(Re^{-3/8})$. This implies a strong peak of interactive pressure gradient of $\mathcal{O}(Re^{1/8})$, and by (2.5) there is also a strong σ_p -peak of the same order.

Eq. (2.5) also indicates that the strong interactive σ_p -peak must be in a tangential direction perpendicular to the interactive pressure gradient. Thus, in two-dimensional or rotationally symmetric flow, the interactive σ_p -peak is simply along the \mathbf{e}_z or \mathbf{e}_{θ} (in cylindrical coordinates) direction; but in a generic three-dimensional flow, as the separation line becomes a skin-friction line (a $\boldsymbol{\tau}_w$ -line^{||}, e.g., [11]), the interactive σ_p -peak of

^{||} $\boldsymbol{\tau}_w = \mu \boldsymbol{\omega} \times \hat{\mathbf{n}}$ is the skin-friction, with $\hat{\mathbf{n}} = -\mathbf{n}$ being the unit normal out of the wall.

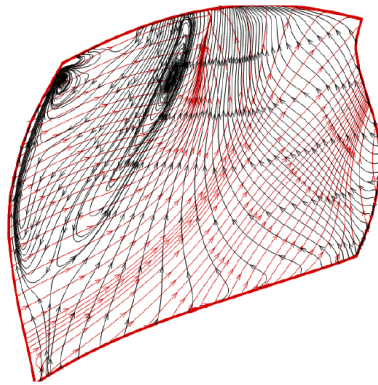


Figure 1: The on-wall vector lines of the skin-friction τ_w (red) and BVF σ_p (black) on the suction side of the rotor blade of a transonic compressor. Notice the strong peak of interactive BVF in the separation zone makes the BVF-lines turn to be basically aligned to the skin-friction lines there.

$\mathcal{O}(Re^{1/8})$ turns to be basically aligned to the τ_w -line direction (plus an $\mathcal{O}(1)$ correction due to the ambient pressure gradient which may have a component perpendicular to τ_w). This (σ_p, τ_w) alignment occurs only in the narrow separation zone. Fig. 3 exemplifies this situation on the suction surface of the rotor blade of a transonic axial compressor. In the figure, the narrow positive BVF peak was found to be caused by shock-boundary layer interaction, which confirms the dual role of σ_p for pinpointing

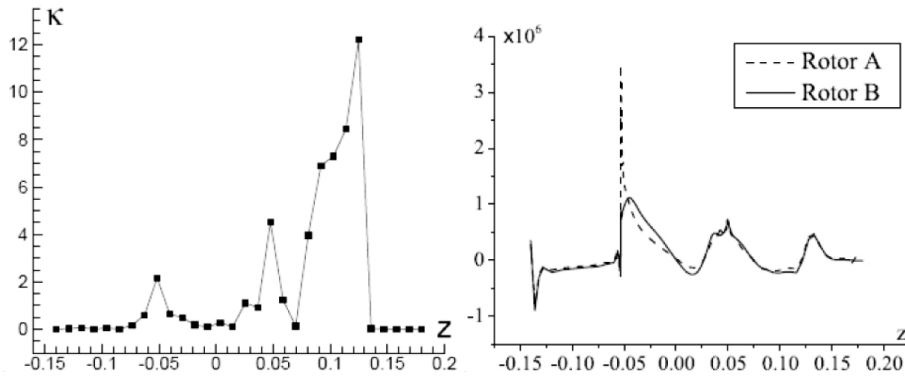


Figure 2: (Left) The hub curvature of a compressor rotor (Rotor A). (Right) Dashed line: The hub BVF of Rotor A. Solid line: the hub BVF of Rotor B, which was reshaped from rotor A to ensure a milder curvature variation.

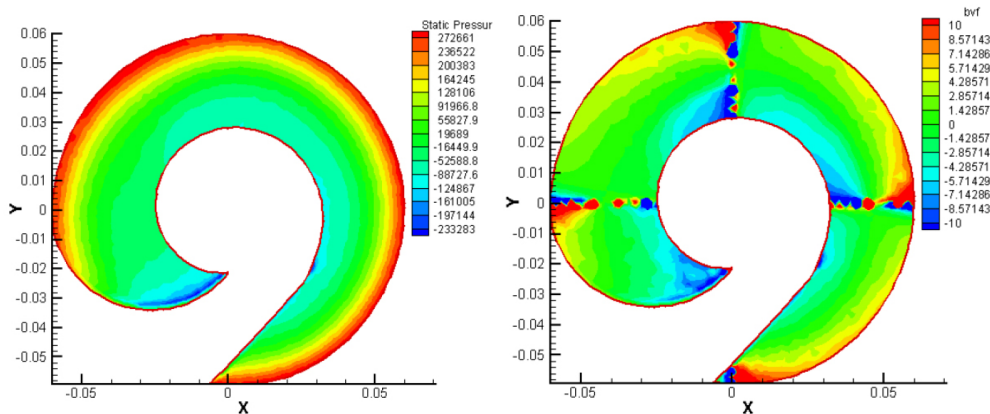


Figure 3: Axial view of the distributions of pressure (left) and boundary vorticity flux (right) over the inducer surface of a high-speed centrifugal pump. Only the latter can reveal the physical root of the cracks. Courtesy of Z. H. Xu [17].

both strong compressing process and strong shearing process on the wall. Note that the τ_w -line convergence seen in the figure, which was the separation criterion proposed by Lighthill [6], is insufficient to identify whether the entire boundary layer is separating; but the above (σ_p, τ_w) alignment criterion does.

The two- and three-dimensional triple-deck structure can appear in much broader situation than boundary layer separation. It also occurs at places where the wall curvature has discontinuities, even if the flow remains attached [2, 7]. This causes $\mathcal{O}(Re^{1/8})$ BVF peaks as well that are often unfavorable, and should be taken into the consideration of flow diagnosis. Fig. 2 shows a correlation of strong BVF peaks identified by RANS-simulation and wall curvature discontinuities along a compressor hub. A more remarkable example is the inducer blade in a high-speed centrifugal pump, on which the computed smooth pressure distribution predicts no trouble but the BVF does, see Fig. 3. The three narrow radial BVF peaks correspond to the places of blade curvature discontinuities, which caused cracks. Once the curvature was made continuous the crack problem disappeared.

4 Force and moment in terms of BVF

We mentioned in § 1 that the pressure distribution (a “global” picture) does not reflect local dynamics, but its gradient (a local picture) does. We now consider the lift on an airfoil contour C in two-dimensional steady flow with $u=Ue_x$ at $x=-\infty$, to show how physically the lift expression in the global picture is cast to that in the local picture. Introduce a coordinate system (n, t, e_z) moving along C , where $t ds$ is the line element of C in clockwise direction so that (n, t, e_z) form a righthand orthonormal triad. Assume the airfoil is sufficiently thin so that it can be represented by its centerline

$$y = \eta(x), \quad 0 \leq x \leq c. \tag{4.1}$$

Denote the upper and lower surfaces of the airfoil by the $+$ and $-$ signs (cf. Fig. 4), and the jump of any function f across the centerline by $\llbracket f \rrbracket$. Let $l(x)$ be the arc-length along the airfoil, such that $dl=dx \sqrt{1 + \eta'^2(x)}$, with $dl=\pm ds$ on the \pm sides. Moreover, let \hat{n} be the unit normal of the airfoil pointing out of the upper surface, i.e. $\hat{n}=-n^+=n^-$. When $Re \gg 1$ the shear stress can be neglected. Thus by the thin-wing theory and the Kutta-Joukowski lift theorem there is**

$$L = \oint p n_y ds = - \int_0^c \llbracket p \rrbracket dx = -\rho U \Gamma_c, \quad \Gamma_c = \int_0^c \gamma(x) dx, \tag{4.2}$$

where γe_z is the strength of the bound vortex sheet as in the classic circulation theory.

Introduce now the *partial lift* $L(x)$ and *partial circulation* $\Gamma(x)$ up to any $x \in [0, c]$:

$$L(x) \equiv - \int_0^x \llbracket p \rrbracket dx = -\rho U \int_0^x \gamma(\xi) d\xi = -\rho U \Gamma(x). \tag{4.3}$$

**By definition, on the (x, y) plane $\Gamma > 0$ if the vorticity is along the e_z direction, i.e., the circulation is counterclockwise.

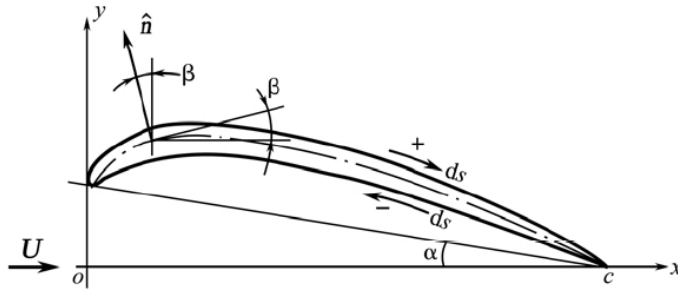


Figure 4: Two-dimensional flow over a thin airfoil.

Then since for BVF we have $\sigma = \sigma_p = \partial p / \partial s$, it follows that

$$U \frac{d^2 \Gamma(x)}{dx^2} = U \frac{d\gamma(x)}{dx} = \frac{d[[p]]}{dl} \frac{dl}{dx} = 2\bar{\sigma} \sqrt{1 + \eta'^2(x)}, \tag{4.4}$$

where $\bar{\sigma}_p \equiv (\sigma_p^+ + \sigma_p^-) / 2$. This equation reveals the explicit dependence of the partial lift and circulation of a thin airfoil on the sum of the BVF on both surfaces, which casts (4.2) to a double integral of BVF moment:

$$L = -2\rho \int_0^c dx \int_0^x \bar{\sigma}_p(\xi) \sqrt{1 + \eta'^2(\xi)} d\xi. \tag{4.5}$$

However, since

$$\frac{d}{dx} [x\gamma(x)] = \gamma(x) + x \frac{d\gamma(x)}{dx}, \quad \gamma(0) = \gamma(c) = 0,$$

by the familiar integration-by-parts formula

$$\int_a^b f(x) dx = [xf(x)]_a^b - \int_a^b xf'(x) dx, \tag{4.6}$$

and using (4.4), (4.5) is reduced to a single integral:

$$L = 2\rho \int_0^c x \bar{\sigma}_p \sqrt{1 + \eta'^2(x)} dx = \rho \oint x \sigma_p ds, \tag{4.7}$$

which is the desired BVF-based lift expression in terms of the x -moment of σ_p . Note that since $p^+ = p^-$ or $\gamma = 0$ at $x = c$, the σ_p distribution is constrained by

$$2 \int_0^c \bar{\sigma}_p \sqrt{1 + \eta'^2(x)} dx = \oint \sigma_p ds = 0. \tag{4.8}$$

The distributions of pressure and BVF over a helicopter rotor airfoil VR-12 at $\alpha = 6^\circ$ are compared in Fig. 5. The lift can be measured by either the area enclosed by the pressure curve or the x -moment of BVF peaks. The latter is highly localized.

The general BVF-based force and moment expressions are derived from the conventional ones in global picture by the so-called *derivative-moment transformation* (DMT),

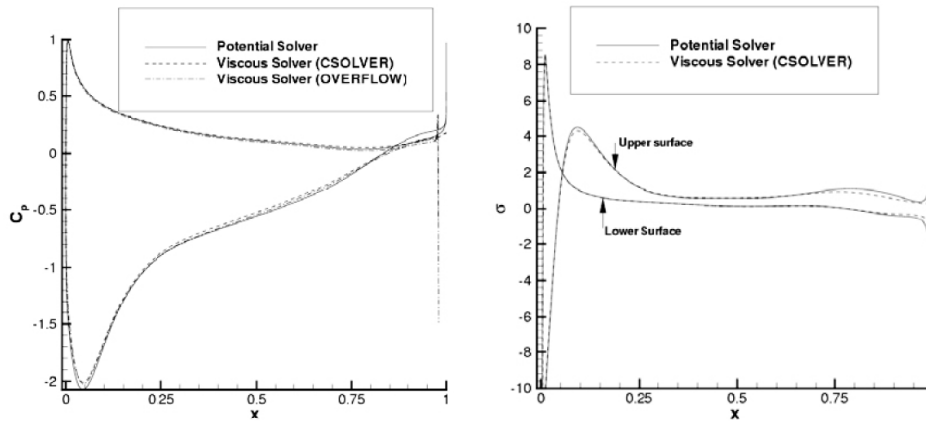


Figure 5: Distributions of p (left) and BVF (right) over airfoil VR12 at $\alpha=6^\circ$, computed by both potential flow theory and NS solvers. Courtesy of Dr. F. L. Zhu [21].

which are the extension of (4.6) to higher dimensions. There have now been a variety of DMT-based alternative total force and moment formulas in terms of local structures (cf. [10, 11, 18]), but only the BVF-type formulas can cover the case with open solid boundary, say S , which has a boundary loop ∂S . This property is important as frequently encountered in practical applications, for example when one wishes to estimate the force on the wing part mounted to a fuselage or a rotor blade mounted on a hub. In what follows we drop the small viscous force as we commonly do in flow management. Then for an n -dimensional flow ($n=2, 3$) over an arbitrarily moving and deforming open solid surface S , the BVF-based force formula reads

$$F = -\frac{\rho}{n-1} \int_S \mathbf{x} \times \sigma_p dS + \frac{1}{n-1} \oint_{\partial S} \mathbf{x} \times p dx, \tag{4.9}$$

of which (4.7) is the lateral component in two-dimensional flow. Similarly, for both $n=2$ and 3, the total moment reads

$$M = \frac{\rho}{2} \int_S x^2 \sigma_p dS - \frac{1}{2} \oint_{\partial S} x^2 p dx. \tag{4.10}$$

5 BVF-embedded airfoil and rotor blade design

Eq. (4.7) for the airfoil lift may exemplify how to incorporate the local-dynamics information in optimal configuration design. It is convenient to locate the origin of the x -coordinate at the mid-chord point; then whether a BVF peak has favorable or unfavorable effect on L is simply determined by the sign of $x\sigma_p$. Moreover, an optimal design would be to enhance positive $x\sigma_p$ and suppress negative $x\sigma_p$ as much as possible, under the condition (4.8) and other conventional constraints. For example, the positive peak at front part of VR-12 airfoil (Fig. 5 (right)) should be suppressed, which by (4.8) will likely lead to a favorable positive BVF on the rear part. This is in full

consistency with keeping the boundary layer attached in as wide range of angles of attack as possible. Therefore, as a general rule: The local-dynamics diagnosis can add a local criterion to the common objective function of integral type in optimal design.

So far no general-purpose optimal design scheme has been developed with embedded BVF constraint. The above rule has to be implemented case by case. For example, to improve the stall performance of VR-12, Zhu [21] employed a simplified inverse design approach using sequential quadratic programming (SQP) method, and set the objective function as

$$f(c_i) = \sigma_{pk_U} + d_0\sigma_{pk_L} + d_1C_l, \quad (5.1)$$

where c_i are the coefficients of the series expansion of airfoil geometry, σ_{pk_U} and σ_{pk_L} are the peak-value BVF segments at upper and lower surfaces, respectively, C_l is the lift coefficient, and d_0 and d_1 are weighting parameters. The result of optimization is shown in Fig. 6. All the excellent performances of VR-12 airfoil for the angles of attack before stall are retained, but the stall angle of attack α_{stall} and maximum lift coefficient C_{lmax} are increased.

A significant improvement of the performance of the aforementioned axial compressor rotor can be gained by applying BVF-based optimal design to fully three-dimensional rotor blade in viscous flow. To enhance the power input to the fluid by the rotor, we maximize the axial moment acting on the blade by the fluid, which is the negative value of the axial component of (4.10) in cylindrical coordinates:

$$M_z|_{to \text{ fluid}} = -\frac{1}{2} \int_S \rho r^2 \sigma_{pz} dS + \frac{1}{2} \oint_{\partial S} p r^2 dz. \quad (5.2)$$

The rotor blade surface S can be treated open at both its root and tip, where the line integral is dominant. The integral of $\rho r^2 \sigma_p$ alone in (5.2) over the middle part of S does not equal the common pressure moment integral. Thus, a simple (and yet partial) implementation of embedding a BVF constraint in optimal-design code could be maximizing this integral alone for a set of discrete sectional foils at different r in the middle part of S , and maximizing both integrals in (5.2) only for the tip and root sectional foils. This strategy was adopted by the second and third authors of the present paper (H. and Q.S.) on a self-developed optimal design RANS code to enhance M_z . The strategy establishes a direct link between the foil parameters and their objective functions at every section, which accelerated the convergence of iteration. But this strategy cannot optimize the leading-edge curve itself in the three-dimensional space.

This scheme has been applied to a transonic compressor, which resulted in an increment of M_z by 6%. Fig. 7 compares the distributions of σ_{pz} on the suction side of the blade before and after BVF-based optimization, indicating that an unfavorable narrow peak $\sigma_{pz} > 0$ caused by shock-induced separation is weakened and shrunk, and shifted toward downstream. This implies that the shock and its induced separation was significantly suppressed.

Fig. 8 compares the total-pressure ratios and adiabatic efficiencies before and after optimization. At the peak-efficiency point, the total-pressure ratio and adiabatic efficiency were increased by 5.73% and 1.11%, respectively. Fig. 9 compares the profiles

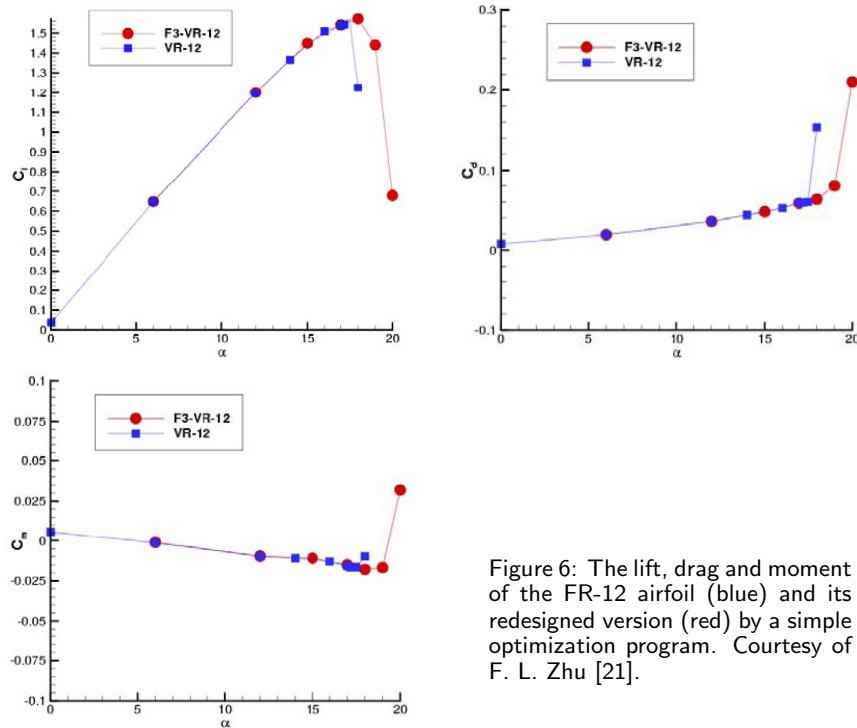


Figure 6: The lift, drag and moment of the FR-12 airfoil (blue) and its redesigned version (red) by a simple optimization program. Courtesy of F. L. Zhu [21].

of these performances at the exit section, indicating that the main improvement occurs at the mid portion of the blade.

Finally, we remark that for given angular velocity of the rotor, maximizing its work rate acting to the fluid implies minimizing the dissipation and energy loss. Ideally, this would be the case if the boundary layers of the shroud, hub and rotor blades could be fully attached, leaving the core flow irrotational and hence effectively inviscid. In particular, in an inviscid and axisymmetric flow model this requires minimizing the azimuthal vorticity ω_θ . This latter criterion has been used by Yang et al. [19] to perform optimal preliminary design of compressor rotor blade. Now the above BVF-based optimal design should also lead to the reduction of ω_θ in the core flow. Our above

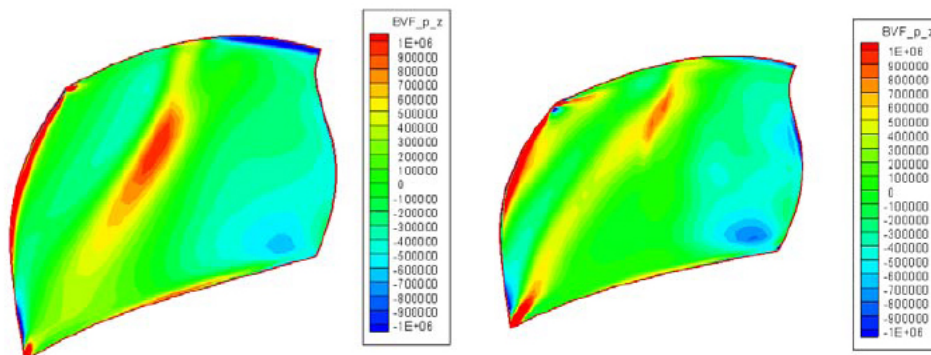


Figure 7: The σ_{pz} contours on the suction side of the original and optimized rotor blades.

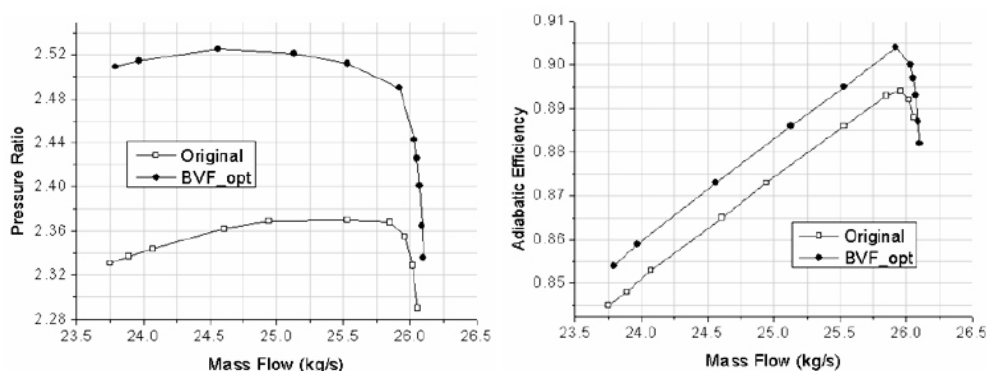


Figure 8: The performance comparison vs mass flux of original and optimized rotor blade.

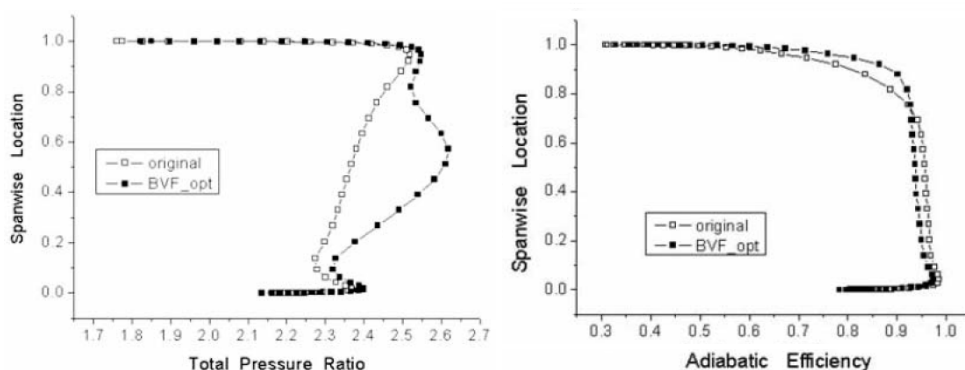


Figure 9: The performance comparison of original and optimized rotor blade at the rotor exit.

3D RANS simulation indicates that the optimal design indeed drives ω_θ toward the shroud and hub (figure not shown), in consistency with the minimum- ω_θ criterion.

6 Concluding remarks

In this paper we present a deeper physical understanding of the concept of the boundary vorticity flux (BVF), demonstrated by a few unpublished or newly worked-out examples. The major points are as follows:

1. The global integrated performance of complex engineering flows is dominated by local dynamic processes and structures that cannot be identified from the primary-variable fields. While quite a few theories have now been available to express global performance in terms of those local structures at different evolution stages inside the flow field, for the purpose of optimal solid-wall configuration design and flow control the on-wall and near-wall local dynamics bears the most direct relevance. The desired on-wall local dynamics is based on the application of proper forms of the Navier-Stokes equation to the solid wall, which for high-Reynolds-number flows is highlighted by the BVF theory.

2. The BVF plays a dual role on the wall. On the one hand, it captures the signature of the compressing process as the local tangent pressure gradient. On the other hand,

it measures the vorticity creation rate and thereby serves as a root of shearing process. This dual role makes the BVF able to pinpoint highly localized wall areas where both processes have strong peaks.

3. Owing to the discovery by the triple-deck theory that whenever the wall boundary conditions have sudden changes a strong but highly localized interactive pressure gradient of $\mathcal{O}(Re^{1/8})$ will appear and be added to the ambient pressure field, the BVF is a faithful marker of boundary-layer separation and the effect of wall-curvature discontinuity. Two examples were given to illustrate the great significance of this role of BVF.

4. When $Re \gg 1$, the total force and moment on a solid surface are commonly considered to be dominated by pressure distribution. By introducing the concept of partial pressure force and circulation, we demonstrate how to transform the common force formula to a double integral of the BVF and then to a single integral of the BVF moment. This provides not only a clear physical interpretation of the general BVF-based force and moment formulas, but also new clue to developing optimal design method with the local dynamics built in as a new constraint. The application of this optimization method was illustrated for the design of a helicopter rotor airfoil and a transonic compressor rotor blade.

Aknowledgments

This work was supported in part by Natural Science Foundation of China, Project No. 10572005. The authors are grateful for valuable discussions with Y. T. Yang, F. Mao and M. Guo.

References

- [1] B.-T. CHU AND L. S. G. KOVASNAY, *Non-linear interactions in a viscous heat-conducting compressible gas*, J. Fluid Mech., 3 (1957), pp. 494–514.
- [2] M. E. GOLDSTEIN AND L. S. HULTGREN, *A note on the generation of Tollmien-Schlichting waves by sudden surface-curvature change*, J. Fluid Mech., 181 (1987), pp. 519–525.
- [3] H. HELMHOLTZ, *Über Integrale der hydrodynamischen Gleichungen, welche den Wirbelbewegungen entsprechen*, J. Reine Angew. Math., 55 (1858), pp. 25–55.
- [4] W. D. HAYES, *Gas Dynamic Discontinuities*, Princeton University Press, 1960.
- [5] L. S. G. KOVASNAY, *Turbulence in supersonic flow*, J. Aero. Sci., 20 (1953), pp. 657–674.
- [6] M. J. LIGHTHILL, *Introduction of boundary layer theory*. In: Rosenhead L. (ed.), *Laminar Boundary Layers*, Oxford University Press, pp. 46–113, 1963.
- [7] K. STEWARTSON, *On laminar boundary layers near corners*, Quart. J. Mech. Appl. Math., 23 (1970), pp. 137–152, (and corrections, 24 (1970), pp. 387–389).
- [8] C. TRUESDELL, *The Kinematics of Vorticity*, Indiana University Press, 1954.
- [9] C. J. WU, L. WANG AND J. Z. WU, *Suppression of the von Kármán Vortex street behind a circular cylinder by a traveling wave generated by a flexible surface*, J. Fluid Mech., 574 (2007), pp. 365–391.

- [10] J. Z. WU, X. Y. LU AND L. X. ZHUANG, *Integral force acting on a body due to local flow structures*, J. Fluid Mech., 576 (2007), pp. 265–286.
- [11] J. Z. WU, H. Y. MA AND M. D. ZHOU, *Vorticity and Vortex Dynamics*, Springer-Verlag, 2006.
- [12] J. Z. WU, R. L. ROACH, C. F. LO, F. L. ZHU, R. M. DOWGWILLO, L. B. JIANG AND R. W. TRAMEL, *Aerodynamic diagnostics based on boundary vorticity dynamics*, AIAA Paper 99-3103, (1999).
- [13] J. Z. WU AND J. M. WU, *Interaction between a solid surface and a viscous compressible flow field*, J. Fluid Mech., 254 (1993), pp. 183–211.
- [14] J. Z. WU AND J. M. WU, *Vorticity dynamics on boundaries*, Adv. Appl. Mech., 32 (1996), pp. 19–275.
- [15] J. Z. WU AND J. M. WU, *Boundary vorticity dynamics since Lighthill's 1963 article*, Theor. Comput. Fluid Dyn., 10 (1998), pp. 459–474.
- [16] J. Z. WU, Y. T. YANG, Y.-B. LUO AND C. POZRIKIDIS, *Fluid kinematics on a deformable surface*, J. Fluid Mech., 541 (2005), pp. 371–381.
- [17] Z. H. XU, *The analysis of impact of three-dimensional unsteady flow in high-speed pump*, Ph.D. Thesis, Tsinghua University, Beijing, 2003.
- [18] Y. T. YANG, R. K. ZHANG, Y. R. AN AND J. Z. WU, *Steady vortex force and slender wing flow diagnosis*, Acta Mech. Sinica, 23 (2007), pp. 609–619.
- [19] Y. T. YANG, H. WU, Q. S. LI, S. ZHOU AND J. Z. WU, *Vorticity dynamics in axial compressor flow diagnosis and design*, J. Fluid Enging., 130 (2008), 041102.
- [20] H. ZHAO, J. Z. WU AND J. S. LUO, *Turbulent drag reduction by traveling wave of flexible wall*, Fluid Dyn. Res., 34 (2004), pp. 175–198.
- [21] F. L. ZHU, *Applications of boundary vorticity dynamics to flow simulation, airfoil design, and flow control*, Ph.D. Dissertation, University of Tennessee, Knoxville, 2000.